Journal of Low Temperature Physics (2024) 214:182–189
https://doi.org/10.1007/s10909-023-03037-2

Structural and Morphological Characterization of Iridium and Ir/Au Films for Transition Edge Sensors

E. Celasco[1,2] · L. Ferrari Barusso[1,2] · M. De Gerone[2] · G. Gallucci[2] · D. Grosso[1,2] · P. Manfrinetti[1] · K. Niazi[1,2] · L. Repetto[1] · F. Gatti[1,2]

Received: 3 November 2023 / Accepted: 30 December 2023 / Published online: 30 January 2024
© The Author(s) 2024

Abstract

Superconducting Transition Edge Sensors employed in X-ray astrophysics space missions were realized and fully characterized in the Low temperature detector laboratory at UniGe. Several samples of Ir and Ir/Au bilayer films were grown by pulsed laser deposition at different deposition rate, varying thickness and resulting variability in critical temperature (Tc) was observed. In particular, we noticed two classes of films having discrete critical temperature (Tc), one at about the critical temperature of the bulk Ir and one at around 1.6 times compared to the bulk. Structural characterization was made and interesting correlation between critical temperature (Tc) and deposition conditions were found. Detailed X-Ray Diffraction investigations suggest a possible explanation of this effect with a clear correlation between microstrain value, grain size, and critical temperatures of the films. The study has been carried out to optimize the specified conditions to grow the film under which it is possible to accurately predict the critical temperature (Tc) by analyzing the X-ray diffraction patterns of Ir/Au films.

Keywords Critical temperature (Tc) · Superconductive edge sensor · X-ray diffraction · Structural analyses

1 Introduction

Highly innovative cryogenic anti-coincidence detectors based on the superconductivity phase transition: iridium-based TES are employed for the X-rays detection in the Advance Telescope for High Energy Astrophysics (ATHENA) mission [1, 2]. In order to meet the stringent requirements of the mission, preliminary accurate

✉ E. Celasco
edvige.celasco@unige.it

1 Università di Genova, 16146 Genoa, Italy

2 INFN Genoa, 16146 Genoa, Italy

characterizations of the Iridium and Iridium Gold films are necessary [3]**.** The quality of the superconducting film, its morphological properties and structural characteristics play a fundamental role, for the accurate determination of the critical temperature (*T*c). The sub-surface mechanism such as underlying variability in micro-structure and morphology, including the crystalline structure of the films, orientation, grain sizes, and the stress induced by lattice mismatches with the substrate vitally attribute to the final value of critical temperature (*T*c).

In this study we report the structural analysis of Ir and Ir/Au bilayer films grown by pulsed laser deposition (PLD) for the fabrication of Superconducting Transition Edge Sensors (TESs) for the application in cryogenic detectors. Two different families of samples with a high *T*c (180 mK) and low *T*c (130 mK) were found. A detailed investigation of the structural properties of these two classes of film transitions showed a strong correlation between a tensile strain, of the reticular lattice, in the high *T*c samples, with a consequent increase in the correspondent *T*c. A shift in structural spectra of Ir and Ir/Au film is evident of structurally induced variation in critical temperature (*T*c). Also, the grain dimensions of the bare film, at higher *T*c, were calculated to be bigger as compared to the low *T*c family.

2 Experimental

All the Iridium films included in this study were grown by pulsed laser deposition (PLD, system) on Silicon substrate having orientation Si(100) with high resistivity ($\rho > 10{,}000\ \Omega$m). Before the deposition of Ir, standard cleaning procedure was followed. All the silicon substrates were carefully cleaned with standard RCA process (sequence of dilute water baths of NH4OH, HF, HCl) to get rid of organic and metallic residues. During the Iridium deposition a PLD (Pulsed Laser Deposition) system of an Nd:YAG (Neodymium-doped Yttrium Aluminum Garnet) infrared laser was employed having a wavelength of 1064 nm, with pulse emission of 10 ns and output energy of 750 mJ at a repetition rate of 10 Hz. Several samples of Ir films were grown by PLD system as mentioned before, on Si substrate, was followed by gold film, in situ deposition. Gold film of desired thickness was deposited in situ by electron beam (e-Beam). The final thickness of the film was checked by an interferometric optical profilometer, and with a Field Emission Scanning Electron Microscope (FESEM), combined with Focused ion beam (FIB) system. To this purpose, cross sections were obtained by ion milling with FIB a section view to investigate with FESEM with secondary electron. (CrossBeam 1540xb, Carl Zeiss AG, Oberkochen, Germany). The as prepared samples were subjected to a number of characterizations, i.e., final thickness of the film, critical temperature (*T*c) and structural and morphological analysis and its electronics properties. The film resistance was measured at 100 mK in a He-3/He-4 dilution refrigerator (Oxford Instrument Kelvin ox 25). The structural measurements, by X-ray Diffraction, were made with X-ray beam produced by copper cathode (Bruker D4 Endeavor) having wavelength $\lambda = 0.15046$ nm from a Cu-Kα source. A detailed discussion on the characterization of the film samples is given next.

3 Discussion/Results

After gold metallization resulting variation in critical temperature (*T*c) was observed, due to the proximity effect, two different clusters are formed clearly. The first cluster corresponds to the original bare film, with a transition temperature at 180 mK; whereas, the second cluster transitions at 130 mK. In the future, the samples with Tc at 180 mK will be indicated with high Tc family, while the one at 130 mK, with low Tc family.

In Fig. 1. Tc versus ratio of Ir/Au film give us a clear indication of the two different families, where black triangle symbols correspond to the high Tc samples, red dot symbols refer to the low Tc samples. After a cross check of the film quality and its thickness with FESEM, a tentative explanation of this behavior was found in the structural characteristics of the film investigated by the X-ray diffraction (XRD). The following Fig. 2 shows a typical XRD spectra of Ir/Au film of the high Tc family that we deposited on the Si substrate (panel a). The XRD spectra show the characteristic reflection line Si (400); whereas, Ir films grow with a preferred structure (111), along with sub-structures (110) and (311), Ir (222), with gold characteristic peaks as Au (111) and Au (222). An example of the shift occurred on Ir (222) peak is shown in the panel (b) where one sample from the high Tc family was compared to the one of low Tc family. The same samples (DM 111 and DM 27) are reported in the following Fig. 3. Firstly, the reference on Si(400) peak of the substrate was fixed, in order to avoid shift due to the not complete planarity of the sample during the XRD analyses. Interestingly, shift toward lower degree value in XRD spectra was observed in this representative sample reported in the panel (b) as well as in all samples of high Tc family. It is worth noting that these samples also present a higher tensile strain values, as described in detail in Sect. 4. We focused our attention on a reproducible shift on all the films with a starting transition temperature of the bare Iridium film of 180 mK. This shift is confirmed for both the Ir (111) and Ir (222) peaks. The correlation of the shift obtained on both Ir (111) and Ir (222) XRD peak, is shown in the panel c) where it is reported the shift of Ir(222) versus Ir(111) peaks

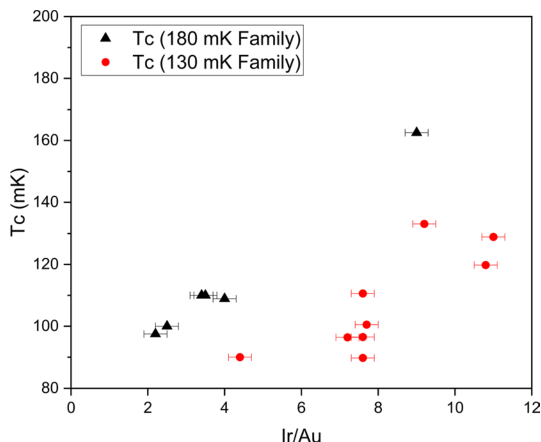

Fig. 1 Dark triangles correspond to proximity effect for the high Tc family, red circles indicate the low Tc samples. (color figure on line)

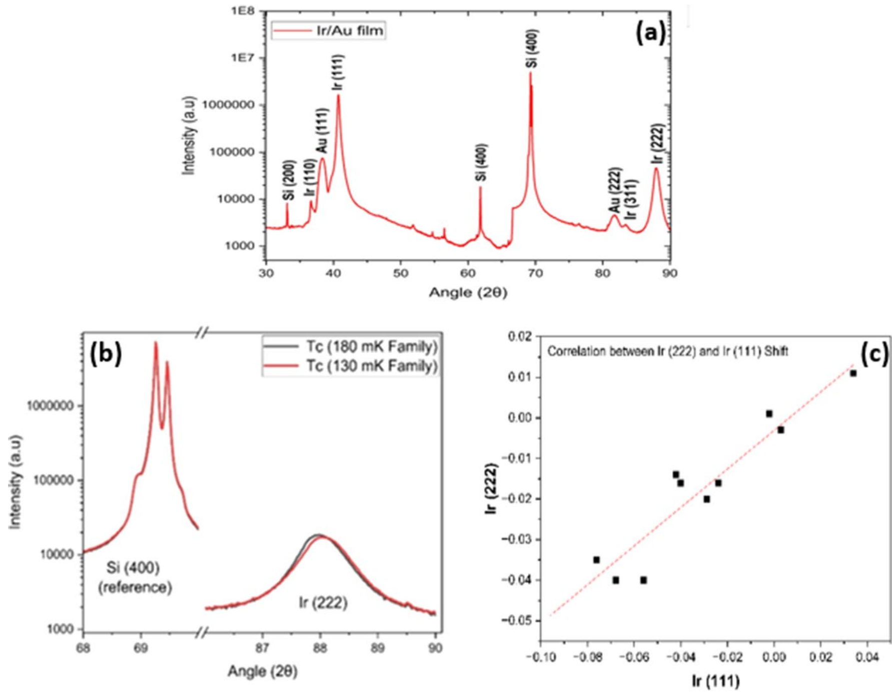

Fig. 2 Panel **a**: Representative XRD Ir/Au spectrum; panel **b**: XRD representative shift on Ir (222) peak of high Tc (black) and low Tc (red); **c** correlation between Ir (222) and Ir (111) shifts. (color figure on line)

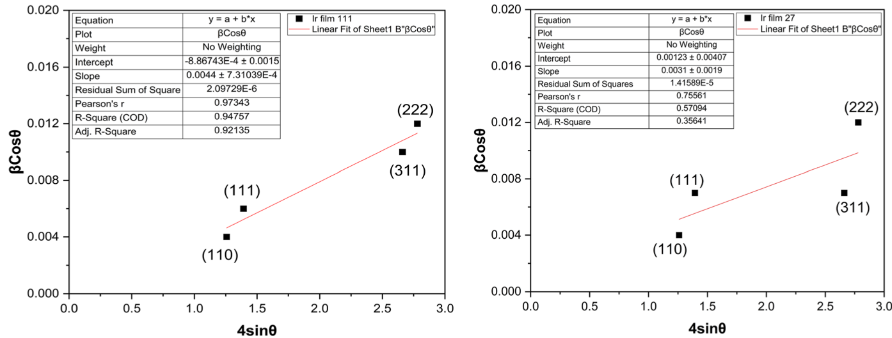

Fig. 3 Shows plot of the fit of Ir(110), Ir(111), Ir(311), Ir(222). In the left panel higher slope give an indication of higher value of microstrain respect to the right panels plot. (color figure on line)

of all samples. A similar shift was found the first time, in our previous work [4], on Titanium-based bolometer.

4 Williamson–Hall (W–H)

Thanks to the W–H method is it possible to estimate the kind of strain (compressive or tensile) of each sample and calculate a direct quantitative evaluation of the micro-strain parameter.

The W–H method works best for isotropic materials, so anisotropy probably makes some peaks wider than others. The W–H method assumes that the line broadening is isotropic, i.e., independent of direction along which they are measured.

All XRD Ir peaks were fitted by Gaussian–Lorentzian—fit with FullPro dedicated XRD data analysis program, and βCosθ versus 4sinθ are plotted in Fig. 3, with Origin software. The equation used for calculation is as follows:

$$\beta \mathrm{Cos}\theta = K\lambda/D + 4\varepsilon \mathrm{Sin}\theta \tag{1}$$

In the above Eq. (1), size of crystallites is represented by D, **ε** is strain in the lattice, K is constant having value 0.9, and wavelength of X-rays λ is 0.15046 nm from a copper Kα radiation source. β is FWHM value and θ corresponds to the Bragg angle of the XRD peaks. Linear fitting was done by plotting βCosθ against 4Sinθ as represented in Fig. 3, where the slope of the linear fitting indicates lattice micro-strain (ε).

With the W–H method it is possible to have a quantitative estimation of the reticular microstrain labeled (ε) in the future [5, 6]**.** We noticed that the microstrain of each sample has a correlation with different final *T*c. The microstrain average value, taking in account all the sample reported in Fig. 1, is 0,0046 for the high *T*c cluster and 0,0036 for the low *T*c one. Herein, higher microstrain parameters (ε) is correlated with higher *T*c samples.

This interesting result allows to correlate higher microstrain value to the bigger Ir(111) or Ir (222) shift in the XRD pattern, of all the high *T*c family samples.

From the positive slope of the fitting value of the W–H method, we can also conclude that our sample presents a tensile strain.

The different lattice constant of IrSi2 respect to Iridium film [7] could produce a tensile strain. The iridium silicate formation is always present when Iridium is grown on Silicon by PLD. In the following Fig. 4, the left panel shows a FESEM estimate of the iridium silicate thickness of a high T_c sample of 30 nm and the right panel shows a representative low T_c sample with a thickness of 19.8 nm.

To avoid the limits of isotropic deformation hypothesis on which W–H method is based, in our future research, more specific methods [8] will be employed to include deformation anisotropy of the sample, which can influence the W–H fitting procedure [9], and give us also the possibility to evaluate the preferred direction of the deformation. The results will be combined with theorical model.

In this work we estimate the grain size (L) with Scherrer formula (L) in both *T*c sample's families. Using the formula represented in the following Eq. 2, where

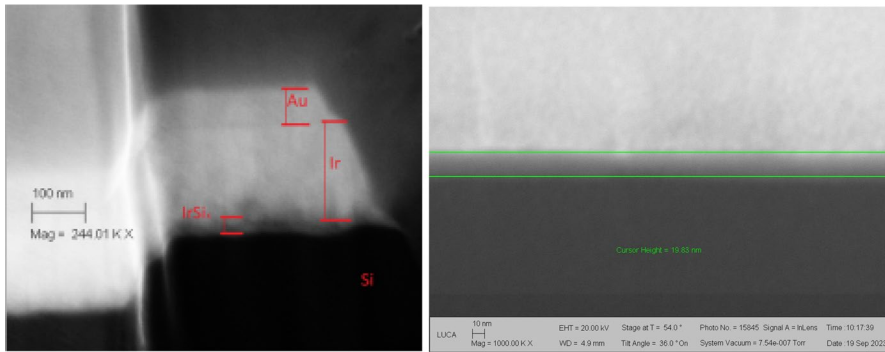

Fig. 4 FESEM for the evaluation of the IrSi thickness in a high Tc sample on the left and of low Tc family on the right panel, the after FIB vertical section view preparation. (color figure online)

$\lambda = 0.15046$ nm is the wavelength of Cu-Kα XRD source, β the FWHM of peak and θ is the diffraction peak angle:

$$L = \frac{0.9\lambda}{\beta \cos(\theta)} \quad (2)$$

An average value for the grain dimension of (111) crystallographic peak of 27 nm was obtained for high Tc family, with respect to the 24 nm grain dimension, calculated for the low *T*c family.

The correlation of grain dimension, microstrain, shift, and critical temperature is clear and reported in Table 1, with the error in the last digit.

The main difference in the deposition conditions between the two sample families lies in the positioning of the laser pointer on the Iridium target relative to its center point. The "high Tc family" samples were grown with the laser directed at the Iridium target, positioned 2.5–3.5 mm off-center. Whereas, the "low Tc family" samples were deposited with the laser aimed at the Iridium target, located 4–5 mm off-center. Also we noted a difference in the thickness of IrSi layer in the two families. The observed difference in IrSi layer thickness is hypothesized to be related to the difference of laser plume conditions during the deposition of the two sets of samples. Specifically, the deposition conditions (such as laser positioning) may have influenced the temperature of the laser plume, leading to variations in the thickness of the resulting IrSi layer.

Table 1 Correlation between higher *T*c values and higher microstrain, XRD and average grain dimension

Samples family	Microstrain (average)	Shift (average) (2Θ)	Average grain size referred to Ir (111) (nm)
High T_c	00046 (1)	006 (1)	27 (1)
Low T_c	00036 (1)	001 (1)	24 (1)

In order to confirm and try to tune the previously described Tc variation between two values on the bare Iridium film, correlated to the microstrain, one possibility, is to induce an external controlled stress, patterning the Iridium film by focused ion beam, with different density matrix of air pillars.

5 Conclusions and New Perspectives

In the as reported study, we confirmed the replication of two sample populations of Ir/Au films grown on Si (100) substrate labeled as a high Tc (180 mK) family and low Tc (130 mK) family, with better understanding of the underlying phenomenon by structural investigations. Different thickness of Au film has proximity effect evident by the decreasing Tc. The Structural characterization by X-ray diffraction revealed a correlation between, compressive microstrain value, crystal size and Tc. The results are reproducible on several samples and with different XRD analyses such as Scherrer and Williamson–Hall methods. It is clearly evident that larger XRD shift, grain size and microstrain correspond to a higher Iridium critical temperature. Future works will be the study of the electrical superconductive characteristics induced by lattice stress modification by FIB.

Acknowledgements The authors would like to thank Mrs M. Rigano of the University of Genova, Mr. L. Parodi, Mr A. Bevilacqua and Mr F. Siccardi of INFN of Genova for their work and the technical support. This works is supported by Italian Space Agency (ASI) grant 2019-27-HH.0

Author contributions E.C, L.F.B, K.N wrote the main manuscrip text and analyzed dataE.C, L.F.B, K.N F.G. have fabricated the samples and made measurements at low TL.R. P.M. F.G revieved technical aspects and made morphological and structural analysesD.G, G.G, M.D.G. have contributed to structural measurementsK.N, E.C: prepared figuresall authos reviewed the manuscript

Funding Open access funding provided by Università degli Studi di Genova within the CRUI-CARE Agreement.

Declarations

Competing interests The authors declare no competing interests.

Open Access This article is licensed under a Creative Commons Attribution 4.0 International License, which permits use, sharing, adaptation, distribution and reproduction in any medium or format, as long as you give appropriate credit to the original author(s) and the source, provide a link to the Creative Commons licence, and indicate if changes were made. The images or other third party material in this article are included in the article's Creative Commons licence, unless indicated otherwise in a credit line to the material. If material is not included in the article's Creative Commons licence and your intended use is not permitted by statutory regulation or exceeds the permitted use, you will need to obtain permission directly from the copyright holder. To view a copy of this licence, visit http://creativecommons.org/licenses/by/4.0/.

References

1. M. D'Andrea, K. Ravensberg, A. Argan, D. Brienza, S. Lotti, C. Macculi, G. Minervini, L. Piro, G. Torrioli, F. Chiarello, L. Ferrari Barusso, M. Biasotti, G. Gallucci, F. Gatti, M. Rigano, H. Akamatsu, J. Dercksen, L. Gottardi, F. de Groote, R. den Hartog, J.W. den Herder, R. Hoogeveen, B. Jackson, A. McCalden, S. Rosman, E. Taralli, D. Vaccaro, M. de Wit, J. Chervenak, S. Smith, N. Wakeham, J. Low Temp. Phys. (2022). https://doi.org/10.1007/s10909-022-02786-w
2. M. Biasotti et al., J. Low Temp. Phys. **199**, 225–230 (2020). https://doi.org/10.1007/s10909-020-02348-y
3. E. Celasco, L. Ferrari Barusso, M. De Gerone, G. Gallucci, D. Grosso, P. Manfrintetti, L. Repetto, M. Schott, F. Gatti, IEEE Trans. Appl. Supercond. **33**, 11 (2023). https://doi.org/10.1109/TASC.2022.3215894
4. B. Siri, E. Celasco, L. Ferrari Barusso, F. Buatier de Mongeot, P. Manfrinetti, G. Manzato, A. Provino, F. Gatti, IEEE Trans. Appl. Supercond. (2021). https://doi.org/10.1109/tasc.2021.3071997
5. M. Qayoom, G.N. Dar, Intl J. Self-Propagating High Temp. Syst. **29**, 213–219 (2020). https://doi.org/10.3103/S1061386220040111
6. B. Yahmadia, N. Kamouna, C. Guaschb, R. Bennaceura, Mater. Chem. Phys. **127**, 239–247 (2011). https://doi.org/10.1016/j.matchemphys.2011.01.066
7. J.W. Arblaster, Platinum Metals Rev. **54**(2), 93–102 (2010). https://doi.org/10.1595/147106710X493124
8. D. Nath, F. Singh, R. Das, Mater. Chem. Phys. **239**, 122021 (2020). https://doi.org/10.1016/j.matchemphys.2019.122021
9. L. Ferrari Barusso, S. Tugliani, M. Fedkevych, E. Celasco, G. Gallucci, D. Grosso, P. Manfrinetti, K. Niazi, F. Gatti, IEEE Trans. Appl. Supercond. **33**(5), 2101104 (2023). https://doi.org/10.1109/TASC.2023.3257822

Publisher's Note Springer Nature remains neutral with regard to jurisdictional claims in published maps and institutional affiliations.